


## Energy and momentum conservation in spin transfer

Alexander Mitrofanov  and Sergei Urazhdin 

Department of Physics, Emory University, Atlanta 30322, Georgia USA

 (Received 4 April 2020; revised 19 October 2020; accepted 20 October 2020; published 3 November 2020)

We utilize simulations of spin-polarized electron scattering by a chain of localized quantum spins to show that energy and linear momentum conservation laws impose strong constraints on the properties of magnetic excitations induced by spin transfer. In turn, orbital and spin dynamics of conduction electrons depends on the dynamical characteristics of the local spins. Our results suggest the possibility to achieve precise control of spin-transfer-driven magnetization dynamics by tailoring the spectral characteristics of the magnetic systems and of the driving electrons.

DOI: [10.1103/PhysRevB.102.184402](https://doi.org/10.1103/PhysRevB.102.184402)

### I. INTRODUCTION

The advent of spin transfer (ST) effect [1–3] has transformed our understanding of nanomagnetism and spurred multiple applications [4–8]. ST is caused by the interaction of spin currents carried by conduction electrons with the magnetization of magnetic materials, resulting in the absorption of an electron’s spin angular momentum component noncollinear with the magnetization [1,9,10]. The absorbed angular momentum drives magnetization dynamics, which can result in magnetization reversal [11,12], precession [13,14], and other dynamical effects [15,16].

Energy and linear momentum conservation laws play a central role in the dynamical processes in nature. Their role in ST has been analyzed in the classical approximation for the magnetization [17–19], but energy and momentum conservation of the quasiparticles involved in spin transfer, in the de Broglie sense, has remained virtually unexplored. The potential significance of the latter can be illustrated by considering the electron photoemission process, whose outcome is determined not by the wave energy and momentum of light but rather by the Planck’s energy and momentum of light quanta, the photons.

Analogously to photoemission, ST involves interaction between electrons and light in magnetic matter, which becomes hybridized with electron spins forming spin waves. The threshold current for ST-driven magnetization dynamics was initially attributed to the requirement that spin accumulation must exceed the energy  $E_m$  of the spin-wave quanta (magnons) generated by ST [20]. However, the energy of magnons associated with quasiumiform magnetization precession excited by ST is small, and the threshold was identified with the compensation of the dynamical damping by ST [10,11].

Recent studies showed that ST can excite dynamical modes throughout the magnon spectrum [21,22], which spans frequencies  $f_m$  from GHz to THz ranges for common ferromagnets (Fs) [23]. Excitation of high-frequency magnons may play a significant role in the interplay between thermal phenomena and ST [24]. Nonlinear interactions among these high-frequency modes can also profoundly influence ST-induced dynamics [25,26]. ST can also drive magnetic

dynamics in antiferromagnets (AFs) [27–29], where the lowest dynamical frequencies are typically in 100s of GHz or in the THz range [30,31], which may enable ultrafast devices and THz oscillators based on AFs driven by ST [32].

The energies  $E_m = hf_m$  of THz magnons are in the meV range. If energy conservation plays a role in ST, a large electrical bias may be required to provide energy sufficient to generate such magnons. Likewise, linear momentum conservation may impose strict requirements on the momentum of the driving electrons in magnetic nanodevices envisioned to operate with short-wavelength magnons generated by ST [5,33]. However, both energy and momentum of magnons have been neglected in the analyses of ST, which with a few exceptions [34–39] have approximated magnetization as a classical vector field.

Here, we use simulations of spin-polarized electron scattering by a quantum spin chain to show that energy and momentum conservation laws impose significant constraints on the magnetic dynamics, as well as the electron’s orbital and spin dynamics resulting from ST. Our results suggest the possibility to control the characteristics of magnetic excitations generated by ST by optimizing these constraints, which may provide a new route for the development of efficient magnetic nanodevices.

### II. MODEL SYSTEM AND SIMULATION APPROACH

To analyze ST, we consider scattering of an electron wavepacket initially propagating in a nonmagnetic medium by a ferromagnet modeled as a localized 1D spin-1/2 chain. In the tight-binding approximation, this system can be described by the Hamiltonian [37,40]

$$\hat{H} = - \sum_i b|i\rangle\langle i+1| - \sum_j J_{sd}|j\rangle\langle j| \otimes \hat{\mathbf{S}}_j \cdot \hat{\mathbf{s}} + J\hat{\mathbf{S}}_j \cdot \hat{\mathbf{S}}_{j+1} + \mu_B \hat{S}_j^z B, \quad (1)$$

where  $b$  is the electron hopping parameter,  $J$  describes the exchange stiffness of the local spins,  $J_{sd}$  their exchange with

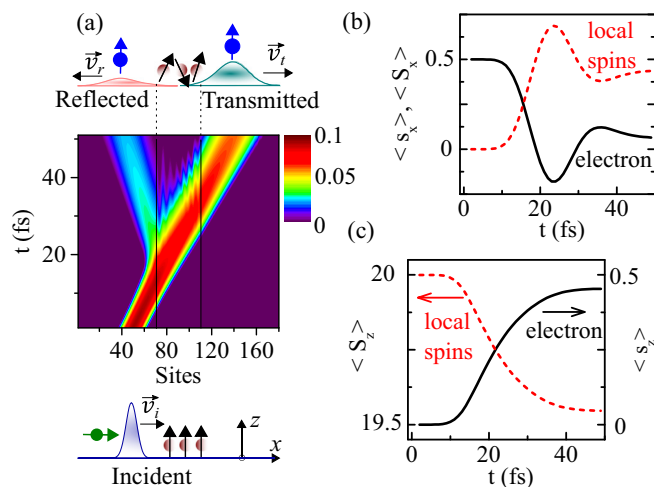


FIG. 1. ST due to scattering of electron wave packet by the chain of 40 spins within 180 tight-binding sites, with  $a = 0.2$  nm,  $b = 1$  eV,  $J = J_{sd} = 0.1$  eV,  $B = 20$  T. (a) Pseudocolor map of wave-packet intensity in the position-time coordinates, for the initial wave-packet polarization along the  $x$  axis. Schematics: The wave packet and the spin chain before and after scattering. The scale unit is the probability per site. (b), (c) Evolution of the expectation values of  $x$  (b) and  $z$  (c) components of electron and chain spins.

the electron,  $B = -B_z$  is the magnetic field, and  $\mu_B$  is the Bohr magneton. The states  $|i\rangle$  are localized on the sites  $i = 1..200$  comprising the entire simulated system that includes the ferromagnet and the nonmagnetic medium surrounding it, forming a complete spatial tight-binding basis for the itinerant electron. The states  $|j\rangle$ , with  $j = 70 - 110$  in our simulations, represent a subset of these sites where the spins-1/2 representing the ferromagnet are localized.  $\hat{s}$ ,  $\hat{S}_j$  are the spin operators of the electron and the local spins. The entire Hilbert space of the system is thus a direct product of the 200-dimensional spatial component of the itinerant electron,  $2d$  spin subspace of this electron, and  $2^{40}$ -dimensional spin subspace of the localized spin-1/2's. However, the dimensionality of the latter subspace in our simulations could be substantially reduced by explicitly taking into account the axial rotational symmetry of the Hamiltonian [40]. We use periodic boundary conditions for both the electron and the spin chain to avoid spurious effects of reflections at the boundaries. Spin-orbit interaction is neglected in our model.

To analyze ST, the system is initialized with the electron forming a Gaussian wave packet spin polarized along the  $x$  axis, while the local spins are in their ground state aligned with the  $z$  axis. The system is then evolved according to the Hamiltonian Eq. (1). The wave packet is partially reflected and partially transmitted by the local spins [Fig. 1(a)]. One can clearly identify the time intervals when the wave packet is localized mostly outside or inside the spin chain, allowing us to analyze the effects of scattering by tracking the time evolution.

### III. SIMULATION RESULTS AND ANALYSIS

To analyze the evolution of each subsystem, we introduce the density matrices  $\hat{\rho}_e = \text{Tr}_m \hat{\rho}$  and  $\hat{\rho}_m = \text{Tr}_e \hat{\rho}$  for the

electron and the local spins, respectively, by tracing out the full density matrix  $\hat{\rho}$  with respect to the other subsystem [37]. The expectation value of an observable  $\hat{A}$  associated with the electron is  $\langle \hat{A} \rangle = \text{Tr}(\hat{A} \hat{\rho}_e)$ , while the probability of its value  $a$  is  $P_a = \langle \psi_a | \hat{\rho}_e | \psi_a \rangle$ , where  $\psi_a$  is the corresponding eigenstate. Similar relations hold for the observables associated with the local spins. For instance, the expectation values of different contributions to the system's energy discussed below were obtained by using the corresponding terms in the Hamiltonian Eq. (1) as  $\hat{A}$ . The distribution of momentum  $p$ , also discussed below, was obtained using the plane-wave eigenstates  $|\psi_k\rangle \sim e^{ikx}$ , defined for the electron and the magnons in the respective spatial domains. Here,  $k = p/\hbar$  is the wave vector describing the corresponding Fourier component of the electron or magnon wave.

Precession of the electron spin around the effective exchange field, produced by the local spins aligned with the  $z$  axis, results in the oscillation of its  $x$  component [Fig. 1(b)]. The oscillation rapidly decays due to dephasing, consistent with the ST mechanisms [1, 10]. The  $x$  component of the local spins mirrors this evolution, so the  $x$  component of the total spin is conserved. The contribution of the Zeeman term in Eq. (1) that breaks the spin conservation is negligible on the considered timescales.

The  $z$  component of electron spin increases from zero to almost its maximum value 1/2, with the local spins mirroring this evolution, Fig. 1(c). This transfer of the spin component collinear with the magnetization is consistent with the recently demonstrated nonclassical contribution to ST [36, 37, 40]. Since the constraints imposed by energy and momentum conservation are expected to be general, we do not separate between the two contributions to ST in the analysis below.

The evolution of different contributions to energy is illustrated in Fig. 2(a). The magnetic energy  $E_m$  comprising the Zeeman and the exchange energies of the local spins increases due to their excitation by ST, while the exchange energy  $E_{sd}$  between the local spins and the electron initially decreases due to the increase of the electron's spin-up [majority] component [see Fig. 1(c)]. We note that the effects of the Zeeman field become significant on the time scales comparable to the inverse of the Larmor precession frequency, about 2 ps for the field of 20 Tesla used in our simulations, 2–3 orders of magnitude larger than our typical simulation times. The two subsystems no longer interact after scattering, so  $E_{sd}$  increases back to zero. Since the Hamiltonian is time independent, the total energy of the system is conserved [dashed line in Fig. 2(a)]. The deficit of energy associated with a finite  $E_m$  after scattering is made up by the reduction of the electron's kinetic energy  $E_{hop}$ . This suggests that the relation between the electron's kinetic energy and the magnetic excitation spectrum plays an important role in ST, as confirmed below.

We now analyze the momentum evolution. Defining linear momentum in ferromagnets can be subtle since the canonical momentum of the magnetization motion is not invariant under spin rotations, resulting in terms of the Wess-Zumino type in the action [41, 42]. Here and below, we use the term momentum to refer to the quantum-mechanical momentum  $\hbar k_e$  of electron with wave vector  $k_e$ , or similarly to the momentum  $\hbar k_m$  of magnon with wave vector  $k_m$ . For brevity, we refer

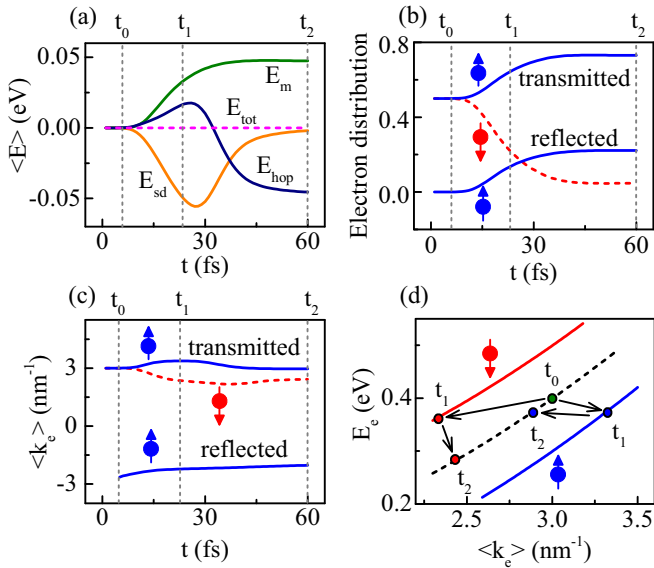


FIG. 2. (a) Evolution of different contributions to energy, as defined in the text. The curves are shifted by the  $t = 0$  values for clarity. (b), (c) Majority (solid curves) and minority (dashed) contributions to the transmitted and reflected wave-packet components (b), and the corresponding average wave vectors (c). The reflected minority component (not shown) is negligible. (d) Energy versus momentum for forward-propagating electron components at times  $t_0$ ,  $t_1$ , and  $t_2$ , as marked in (a), (b). Solid curves: Spin-dependent electron dispersion inside the spin chain; dashed curve: dispersion outside the chain.

below to the wave vector as momentum, since the two quantities are simply related by  $\hbar$ . Before scattering, the wave packet contains only the forward-propagating component, with equal majority and minority spin contributions, Fig. 2(b). During scattering, the minority contribution decreases, while the majority contribution increases, consistent with the transfer of the  $z$  spin component shown in Fig. 1(c). Additionally, a majority-spin backward-propagating component emerges due to the electron reflection by the spin chain. The reflected minority-spin component is negligible in the approximation of the same electron hopping parameter inside and outside the spin chain, consistent with the mechanisms of electron-magnon scattering discussed below.

The momentum of the reflected majority-spin component is considerably smaller than that of the original wave packet [Fig. 2(c)], indicating that electron reflection by the chain involves a large transfer of energy. Meanwhile, the momentum of the majority-spin forward-propagating component increases, and that of the minority component decreases as the electron enters the chain, consistent with the spin splitting of the electronic band structure inside the chain due to the sd exchange [see Fig. 2(d)]. However, the difference between the momenta of the two spin components remains significant even after scattering, indicating that the electron experiences spin-dependent momentum and energy loss. This is confirmed by Fig. 2(d), which shows the average momentum and energy of the forward-propagating components calculated for instants  $t_0$ ,  $t_1$ , and  $t_2$  before, during, and after scattering, as marked in Figs. 2(a) and 2(b). The momentum and the energy of the majority-spin component are slightly reduced at  $t_2$  relative to

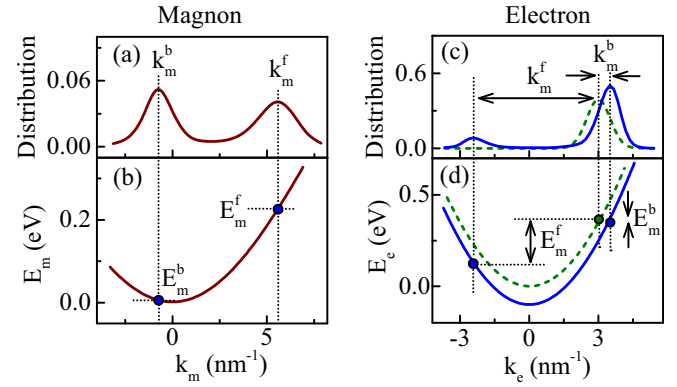


FIG. 3. (a) Momentum distribution of the generated magnons at  $t = t_1$ . (b) Magnon dispersion. (c) Momentum distribution of the majority-spin wave-packet component at  $t = t_0$  (dashed curve) and at  $t = t_1$  (solid curve). (d) Electron dispersion  $E_e = 2b[1 - \cos(k_e a)]$  outside the spin chain (dashed curve) and majority-spin dispersion  $E_{e,\uparrow} = 2b[1 - \cos(k_e a)] - J_{sd}$  in the spin chain (solid curve). The momenta  $k_m^f$ ,  $k_m^b$ , and the energies  $E_m^f$ ,  $E_m^b$  of the forward- and backward-propagating magnon groups are indicated.

$t_0$ , while those of the minority-spin component are significantly reduced.

The variations of the electron's energy and momentum (Fig. 2) are inconsistent with quasielastic scattering, suggesting that the energy and the momentum of the generated magnons play a significant role in the scattering process. This is confirmed by the analysis of the relation between the distribution of the generated magnons and the characteristics of the wave packet, Fig. 3. Two distinct groups of magnons are generated: forward-propagating magnons with a large central momentum  $k_m^f$  and backward-propagating magnons with a small central momentum  $k_m^b$  [Fig. 3(a)]. We use the magnon dispersion relations  $E_m = 4J(1 - \cos(k_m a)) + S\mu_B B$ , where  $a$  is the tight-binding site spacing, to determine the corresponding magnon energies  $E_m^f$  and  $E_m^b$  [Fig. 3(b)].

The relations between the momenta of the generated magnons and the characteristics of the electron wave packet are illustrated in Fig. 3(c), which shows the majority-spin momentum distributions of the wave packet at  $t = t_0$  and at  $t_1$ . The difference between the initial central momentum  $k_e^i$  of the wave packet and the momentum  $k_e^r$  of the reflected component is equal to the momentum  $k_m^f$  of the forward-propagating magnons generated due to ST, while the corresponding difference for the momentum  $k_e^t$  of the transmitted wave packet component is equal to the momentum  $k_m^b$  of the generated backward-propagating magnons.

By analyzing the dispersion of the electron outside the spin chain, as well as the majority-spin dispersion of electron inside the spin chain [Fig. 3(d)], we find that the energy  $E_e^r$  of the reflected component is reduced relative to the initial energy  $E_e^i$  by the energy  $E_m^f$  of the forward-propagating magnons generated by scattering, while the energy  $E_e^t$  of the transmitted component is reduced by the energy  $E_m^b$  of the backward-propagating magnons. Here, the term energy refers to the expectation value of energy of the corresponding quantum-mechanical state rather than the net energy carried by the wave. Thus, generation of forward-propagating

magnons is associated with electron reflection, while generation of backward-propagating magnons—with the forward scattering of electrons, described by the relations

$$E_e^i = E_m^{f(b)} + E_e^{r(t)}, \quad k_e^i = k_m^{f(b)} + k_e^{r(t)} \quad (2)$$

between the energies and the momenta of the quasiparticles involved in the corresponding scattering processes. To confirm our interpretation, we solved these equations using the magnon and the electron dispersions. For instance, the equation for the momentum  $k_e^t$  of the transmitted electron is

$$b - \frac{S\mu_B B - J_{sd} + 4J \cos(k_e^i a - k_e^t a)}{2[\cos(k_e^t a) - \cos(k_e^i a)]} = 0. \quad (3)$$

Its numeric solution is consistent with Fig. 3(c) [40]. The first relation in Eq. (2) describes energy conservation, as expected for the time-independent Hamiltonian Eq. (1). However, its translation symmetry is broken by the spin chain, so the momentum needs not be conserved. Indeed, the momentum of the forward-propagating majority electron becomes reduced after scattering, as expected since its energy is reduced due to magnon generation [see Fig. 2(d)]. However, the generated magnon with momentum  $k_m^b$  propagates backward, i.e., the total momentum is reduced in this process. Nevertheless, the momentum relation in Eq. (2) is governed by the same spatial interference between the spin wave and the incident/scattered electron wave functions as in the momentum-conserving processes, and therefore, for simplicity, we call it the momentum conservation condition. Roughness of the magnetic interfaces can be expected to partially relax the constraints imposed by momentum conservation. However, by analogy to the light reflection from rough surfaces, we expect that these effects become averaged out on the length scales of the wavelengths of magnons generated by ST, which are significantly larger than the atomic-scale roughness of typical interfaces.

#### IV. EFFECTS OF MAGNON DISPERSION ON ELECTRON SCATERING

Electron scattering described by Eq. (2) is governed by the electron and magnon dispersions. Here, we demonstrate one of the consequences—dependence of electron scattering and ST on the magnon dispersion—which is not captured by the models based on the classical approximation for magnetization [40].

Figure 4(a) shows the electron momentum distributions at the instant  $t_1$  for three different values of exchange stiffness  $J$ . The transmitted component is not significantly affected by the variations of  $J$ , as expected since the energy of the magnons with a small momentum  $k_m^b$ , which are generated by the transmitted electrons, is almost independent of the exchange stiffness. In contrast, the magnitude of the momentum of the reflected component rapidly decreases with increasing  $J$ , which is mirrored by the decrease of the momentum  $k_m^f$  of the generated magnons [Fig. 4(b)]. This effect is consistent with the increase of the energy  $E_m^f$  of these large-momentum magnons, resulting in a decrease of the scattered electron's energy. At  $J = 1$  eV, the momentum of the scattered electron becomes close to zero, i.e., all of its initial energy is transferred to the generated magnon.

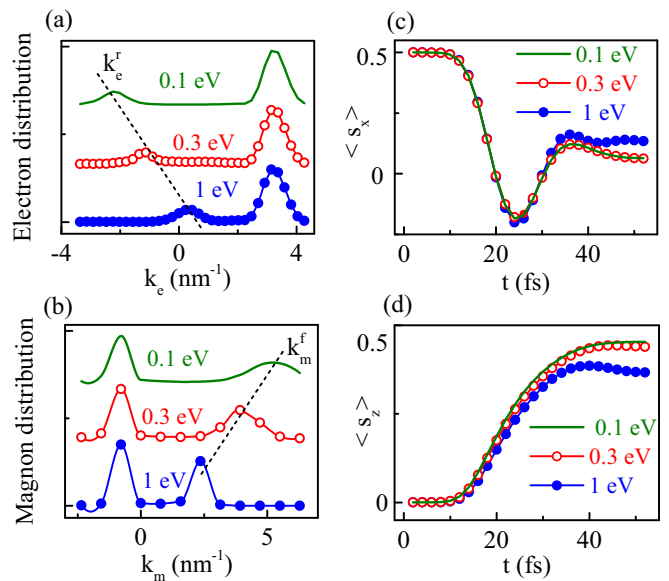


FIG. 4. Effects of magnon dispersion on ST. Electron (a) and magnon (b) momentum distributions at  $t = t_1$ , for the labeled values of  $J$ . Evolution of the  $x$  (c) and  $z$  components of electron spin (d).

The evolution of both the  $x$  and the  $z$  components of the electron spin is similar for  $J = 0.1$  eV and  $J = 0.3$  eV, [Figs. 4(c) and 4(d)]. However, for  $J = 1$  eV, the transfer of both the  $x$  and the  $z$  components of spin is reduced. The electron's energy is no longer sufficient to generate the largest-momentum magnons, resulting in a reduced efficiency of ST. In our simulation, electrons can be scattered into any band states, so this effect of magnon dispersion on ST becomes noticeable only at large  $J$ , when the magnon energies become comparable to the electron band energy. In real systems, the available electron energy is much smaller, as defined by the occupied Fermi surface. Consequently, a significant dependence of electron scattering and spin dynamics on the magnon dispersion can be expected even for modest variations of  $J$  or other parameters controlling the magnon dispersion, such as the magnetic anisotropy or field [40]. We leave analysis of these effects to future studies.

#### V. SUMMARY

To summarize, we have shown that energy and momentum conservation laws define the energies and the momenta of magnons generated in the ST process. As one of the consequences, the spectral distribution of spin waves generated by ST in tunnel junctions must significantly differ from those in metallic systems. The demonstrated relations may provide a path for the development of laserlike magnetic nanodevices, where specific magnetic modes are excited by ST due to the judicious optimization of constraints imposed by the conservation laws.

The demonstrated relations are relevant not only to ST, but also to orbital and the spin dynamics of electrons scattered by the ferromagnets. For instance, electron backscattering at magnetic interfaces, which involves generation of large-momentum magnons, should strongly depend on the available

electron energy. The constraints imposed on spin transfer by the conservation laws are also particularly relevant for AFs, where the characteristic magnon energies are two orders of magnitude larger than in ferromagnets.

## ACKNOWLEDGMENTS

This work was supported by the U.S. Department of Energy, Office of Science, Basic Energy Sciences, under Award No. DE-SC0018976.

- 
- [1] J. Slonczewski, *J. Magn. Magn. Mater.* **159**, L1 (1996).
- [2] L. Berger, *Phys. Rev. B* **54**, 9353 (1996).
- [3] Y. B. Bazaliy, B. A. Jones, and S.-C. Zhang, *Phys. Rev. B* **57**, R3213(R) (1998).
- [4] A. D. Kent and D. C. Worledge, *Nat. Nanotechnol.* **10**, 187 (2015).
- [5] B. Divinskiy, V. E. Demidov, S. O. Demokritov, A. B. Rinkevich, and S. Urazhdin, *Appl. Phys. Lett.* **109**, 252401 (2016).
- [6] N. Locatelli, V. Cros, and J. Grollier, *Nat. Mater.* **13**, 11 (2013).
- [7] J.-V. Kim, *Solid State Physics*, edited by R. E. Camley and R. L. Stamps (Elsevier, Netherlands, 2012), pp. 217–294.
- [8] T. Chen, R. K. Dumas, A. Eklund, P. K. Muduli, A. Houshang, A. A. Awad, P. Durrenfeld, B. G. Malm, A. Rusu, and J. Åkerman, *Proc. IEEE* **104**, 1919 (2016).
- [9] S. Zhang, P. M. Levy, and A. Fert, *Phys. Rev. Lett.* **88**, 236601 (2002).
- [10] D. Ralph and M. Stiles, *J. Magn. Magn. Mater.* **320**, 1190 (2008).
- [11] J. A. Katine, F. J. Albert, R. A. Buhrman, E. B. Myers, and D. C. Ralph, *Phys. Rev. Lett.* **84**, 3149 (2000).
- [12] S. Mangin, D. Ravelosona, J. A. Katine, M. J. Carey, B. D. Terris, and E. E. Fullerton, *Nat. Mater.* **5**, 210 (2006).
- [13] S. I. Kiselev, J. C. Sankey, I. N. Krivorotov, N. C. Emley, R. J. Schoelkopf, R. A. Buhrman, and D. C. Ralph, *Nature* **425**, 380 (2003).
- [14] W. H. Rippard, M. R. Pufall, S. Kaka, S. E. Russek, and T. J. Silva, *Phys. Rev. Lett.* **92**, 027201 (2004).
- [15] V. E. Demidov, S. Urazhdin, and S. O. Demokritov, *Nat. Mater.* **9**, 984 (2010).
- [16] M. Madami, S. Bonetti, G. Consolo, S. Tacchi, G. Carlotti, G. Gubbiotti, F. B. Mancoff, M. A. Yar, and J. Åkerman, *Nat. Nanotechnol.* **6**, 635 (2011).
- [17] P. Yan, A. Kamra, Y. Cao, and G. E. W. Bauer, *Phys. Rev. B* **88**, 144413 (2013).
- [18] S. Dasgupta and O. Tchernyshyov, *Phys. Rev. B* **98**, 224401 (2018).
- [19] G. Tatara and H. Kohno, *Phys. Rev. Lett.* **92**, 086601 (2004).
- [20] M. Tsoi, A. G. M. Jansen, J. Bass, W.-C. Chiang, M. Seck, V. Tsoi, and P. Wyder, *Phys. Rev. Lett.* **80**, 4281 (1998).
- [21] K.-J. Lee, A. Deac, O. Redon, J.-P. Nozières, and B. Dieny, *Nat. Mater.* **3**, 877 (2004).
- [22] M. L. Polianski and P. W. Brouwer, *Phys. Rev. Lett.* **92**, 026602 (2004).
- [23] F. Menzinger, G. Caglioti, G. Shirane, R. Nathans, S. J. Pickart, and H. A. Alperin, *J. Appl. Phys.* **39**, 455 (1968).
- [24] G. E. W. Bauer, E. Saitoh, and B. J. van Wees, *Nat. Mater.* **11**, 391 (2012).
- [25] V. E. Demidov, S. Urazhdin, E. R. J. Edwards, M. D. Stiles, R. D. McMichael, and S. O. Demokritov, *Phys. Rev. Lett.* **107**, 107204 (2011).
- [26] B. Divinskiy, S. Urazhdin, S. O. Demokritov, and V. E. Demidov, *Nat. Commun.* **10**, 5211 (2019).
- [27] T. Jungwirth, X. Marti, P. Wadley, and J. Wunderlich, *Nat. Nanotechnol.* **11**, 231 (2016).
- [28] J. Železný, P. Wadley, K. Olejník, A. Hoffmann, and H. Ohno, *Nat. Phys.* **14**, 220 (2018).
- [29] T. Moriyama, K. Oda, T. Ohkochi, M. Kimata, and T. Ono, *Sci. Rep.* **8**, 14167 (2018).
- [30] J. van Kranendonk and J. H. van Vleck, *Rev. Mod. Phys.* **30**, 1 (1958).
- [31] T. Kampfrath, A. Sell, G. Klatt, A. Pashkin, S. Mährlein, T. Dekorsy, M. Wolf, M. Fiebig, A. Leitenstorfer, and R. Huber, *Nat. Photonics* **5**, 31 (2010).
- [32] R. Khymyn, I. Lisenkov, V. Tiberkevich, B. A. Ivanov, and A. Slavin, *Sci. Rep.* **7**, 43705 (2017).
- [33] D. Grundler, *Nat. Nanotechnol.* **11**, 407 (2016).
- [34] S. Urazhdin, *Phys. Rev. B* **69**, 134430 (2004).
- [35] Y. Wang and L. J. Sham, *Phys. Rev. B* **85**, 092403 (2012).
- [36] A. Zholud, R. Freeman, R. Cao, A. Srivastava, and S. Urazhdin, *Phys. Rev. Lett.* **119**, 257201 (2017).
- [37] P. Mondal, U. Bajpai, M. D. Petrović, P. Plecháč, and B. K. Nikolić, *Phys. Rev. B* **99**, 094431 (2019).
- [38] S. A. Bender, R. A. Duine, and Y. Tserkovnyak, *Phys. Rev. B* **99**, 024434 (2019).
- [39] M. D. Petrović, P. Mondal, A. E. Feiguin, P. Plecháč, and B. K. Nikolić, Spintronics meets density matrix renormalization group: Nonclassical magnetization reversal and entanglement growth due to current-pulse-driven quantum spin torque, [arXiv:2002.04655](https://arxiv.org/abs/2002.04655).
- [40] See Supplemental Material at <http://link.aps.org/supplemental/10.1103/PhysRevB.102.184402> for additional details on simulations and results supporting the analysis in the main text .
- [41] G. E. Volovik, *J. Phys. C* **20**, L83 (1987).
- [42] F. D. M. Haldane, *Phys. Rev. Lett.* **57**, 1488 (1986).